



LAWRENCE
LIVERMORE
NATIONAL
LABORATORY

Two-Color, Intracavity Pump-Probe, Cavity Ringdown Spectroscopy

J. Jiang, A. D. McCartt

April 21, 2021

The Journal of Chemical Physics

Disclaimer

This document was prepared as an account of work sponsored by an agency of the United States government. Neither the United States government nor Lawrence Livermore National Security, LLC, nor any of their employees makes any warranty, expressed or implied, or assumes any legal liability or responsibility for the accuracy, completeness, or usefulness of any information, apparatus, product, or process disclosed, or represents that its use would not infringe privately owned rights. Reference herein to any specific commercial product, process, or service by trade name, trademark, manufacturer, or otherwise does not necessarily constitute or imply its endorsement, recommendation, or favoring by the United States government or Lawrence Livermore National Security, LLC. The views and opinions of authors expressed herein do not necessarily state or reflect those of the United States government or Lawrence Livermore National Security, LLC, and shall not be used for advertising or product endorsement purposes.

Two-Color, Intracavity Pump-Probe, Cavity Ringdown Spectroscopy

Jun Jiang¹ and A. Daniel McCartt^{*1}

¹*Center for Accelerator Mass Spectrometry,*

Lawrence Livermore National Laboratory, Livermore, California 94550, USA

(Dated: March 31, 2022)

Abstract

We report a proof-of-principle demonstration of intracavity pump-probe, cavity ringdown (CRD) detection in a three-mirror, traveling-wave cavity. With cavity-enhanced pump *power* and probe absorption *pathlength*, the technique is a generally-applicable, high-sensitivity, high-selectivity detection method. In our experiments, the pump radiation is switched off during every other probe ringdown, which allows uncorrelated measurements of analyte and background cavity decay rates. The net, two-color signal from the difference between the pump-on and pump-off decay rates is immune to empty-cavity ringdown drifts and spectral overlaps from non-target molecular transitions. The immunity to the ringdown drifts allows longer signal-averaging, and thus higher detection sensitivity. The ability to compensate for the background absorption enhances the detection selectivity in spectrally congested regions. Our technique is well-suited for trace-detection in the mid-IR region, where pump-probe schemes based on strong ro-vibrational transitions can be applied. In this work, two-color CRD detection is implemented on a ladder-type, three-level system based on the N₂O, $\nu_3 = 1 \leftarrow 0$, P(19) (pump) and $\nu_3 = 2 \leftarrow 1$, R(18) (probe) ro-vibrational transitions. By frequency-locking two quantum cascade lasers to the *p*-polarization (pump, Finesse = 5280) and *s*-polarization (probe, Finesse = 67700) cavity modes, we achieve high intracavity pump power (36 W) and high probe ringdown rates (>2 kHz). The observed two-color spectra are simulated by a density-matrix, three-level-system model which is solved under the constraints of the cavity resonance conditions. In addition to its background compensation capability, experimental flexibility in the selection of pump-probe schemes and signal insensitivity to intracavity laser power are further features which enhance the utility of our technique for mid-IR trace-detection.

LLNL-JRNL-821837

* Corresponding author. Email: mccartt1@llnl.gov

I. INTRODUCTION

Cavity ringdown (CRD) spectroscopy is a highly-sensitive, absorption-based detection method which allows accurate quantification of trace concentrations. The technique has been used in a wide range of research areas,¹ such as trace-gas detection, atmospheric sensing, molecular spectroscopy, chemical kinetics studies, and even condensed-phase characterization. The high sensitivity of CRD detection is a result of both cavity-enhanced absorption (i.e. long effective absorption pathlength) and its insensitivity to laser shot-to-shot power fluctuations (because the measured CRD rate is independent of the initial laser intensity). Detection sensitivity better than 10^{-10} cm⁻¹ can be routinely achieved, especially in the visible and near-IR regions, where high-reflectivity mirrors, sensitive detectors, and tunable radiation sources with sufficient output power are all readily available. Recent advances in all three previously mentioned technological areas (i.e. mirror coatings, detectors, and lasers), in particular, the development of compact, room-temperature quantum cascade lasers (QCL), have pushed the application of the CRD techniques into the mid-IR spectral range.² Chemical sensing capability in the mid-IR region is highly desirable, because strong, fundamental-band, ro-vibrational transitions typically lie in this so-called “molecular fingerprint region” (3 – 20 μ m).

Given its immunity to laser intensity fluctuations, shot-noise-limited detection sensitivity is possible with CRD detection. In practice, the presence of both frequency- and time-dependent variations in the empty-cavity decay rates (γ_c) prevents shot-noise-limited sensitivity in most conventional, linear-absorption CRD measurements. A recent breakthrough in the CRD detection sensitivity occurred following the development of the saturated-absorption cavity ringdown (SCAR) method.³⁻⁶ For conventional CRD detection, power saturation is considered an undesirable effect, because a high level of saturation at the beginning of the ringdown leads to a non-exponential decay signal. The SCAR technique utilizes the time-dependent power saturation of the molecular transition during the ringdown event to achieve simultaneous measurement of cavity losses from saturable (molecular absorption with sufficiently large transition dipole moments) and non-saturable (the empty cavity) sources. With the ability to measure the linear, gas-induced absorption rate (γ_g) free from the effects of the fluctuating γ_c , the SCAR method significantly increases the sensitivity of CRD detection. For example, by measuring the ν_3 -fundamental, P(20) transition of

$^{14}\text{CO}_2$ at $4.5\ \mu\text{m}$, the SCAR method achieved ^{14}C quantification at 5 parts-per-quadrillion (ppq) $^{14}\text{C}/^{12}\text{C}$ level,⁶ which is $\sim 60\times$ more sensitive than the minimum ^{14}C concentration measurable by conventional, linear-absorption-based CRD techniques.^{7,8} While accelerator mass spectrometer (AMS) remains the most sensitive analytical tool for ^{14}C quantification (with sensitivity below 1 ppq), the relative simplicity and low cost of mid-IR CRD detection (both linear and SCAR) makes it an attractive alternative ^{14}C quantification method to AMS, especially for biological applications, where detection sensitivity at 1/3 of ^{14}C natural abundance ($^{14}\text{C}/^{12}\text{C}\sim 1200$ ppq) is sufficient.⁷ The demonstration of the feasibility of CRD-based, ^{14}C quantification has spurred the recent development of commercial, QCL-based, linear-CRD ^{14}C sensors.⁹

In trace-detection of polyatomic molecules, due to the high density of ro-vibrational transitions, the ultimate detection limit is not only determined by the detection *sensitivity*, but also the detection *selectivity*, i.e., the ability to detect the target transition in the presence of severe spectral overlaps with transitions from other molecular species.¹⁰ While SCAR detection allows for greater sensitivity over the conventional linear CRD techniques, it does not, in general, lead to improved selectivity, because SCAR detection is still based on one-photon absorption similar to the conventional CRD methods. Enhanced detection selectivity is possible with the SCAR technique only in special cases for which the background molecular absorption is “non-saturated” under the experimental conditions (i.e. the laser excitation rate is significantly slower than the relaxation rate due to collisions and/or radiative decay). In those cases, the γ_g due to the target molecular transition can be determined separately from the total non-saturable cavity loss due to γ_c and the background absorption. This special case, however, does not apply for $^{14}\text{CO}_2$ quantification. Due to the extreme scarcity of $^{14}\text{CO}_2$, even the high hot-band absorption signals (with lower level of the transition in the $5000\ \text{cm}^{-1}$ region) from $^{13}\text{CO}_2$ (1.1% natural abundance) are significantly stronger (by $\sim 1000\times$) than the $^{14}\text{CO}_2$ fundamental transition signals at room temperature. Background absorption from these hot-band transitions cannot be compensated by the SCAR method, because most of these transitions (with $\Delta v_3 = 1$) have similar transition dipole moments as the $^{14}\text{CO}_2$ ν_3 -fundamental transitions. To mitigate severe spectral overlap with hot-band signals from $^{13}\text{CO}_2$ (and $^{12}\text{CO}_2$), the CRD measurements of $^{14}\text{CO}_2$ (linear and saturated-absorption) need to be carried out at low temperatures, which are achieved either by placing the cavity inside a large freezer (250 K),⁷ or cryogenic cooling of the cavity with a Stirling en-

gine (170 K).⁶ The cooling needs for the application of both linear and saturated-absorption CRD detection for ^{14}C quantification not only increase the engineering costs, but also make the CRD detection setup less field-deployable.

With the goal of improving the detection *selectivity* in a spectrally congested region, Lehmann proposed a resonance-enhanced, one-color, two-photon (1C2P) CRD detection scheme,^{10,11} which has been recently implemented by Zhao et. al.¹² on the N_2O molecule. Similar to the SCAR method, 1C2P-CRD detection relies on the high intracavity laser power achieved with a cavity-locked laser. While both one-photon absorption (in the absence of saturation) and empty-cavity decay rates depend linearly on the intracavity power, the two-photon absorption (TPA) rate has a quadratic power dependence. This differential power dependence enables separate measurements of the linear (empty cavity + one-photon absorption) and TPA-induced loss rates from each 1C2P-CRD transient. High sensitivity and high selectivity, room temperature trace-detection is thus possible with this novel technique. However, the detection sensitivity of the 1C2P-CRD method is expected to be species-dependent. For mid-IR trace-detection, which takes advantage of strong $\Delta v = 1$ ro-vibrational transitions, the efficiency of 1C2P excitation relies on the existence of a pair of *linked* fundamental-band ($1 \leftarrow 0$) and “hot-band” ($2 \leftarrow 1$) ro-vibrational transitions with similar transition frequencies. If these two transition frequencies are sufficiently close, the transition probability of the overall, $2 \leftarrow 0$, two-photon transition is resonance-enhanced. For example, in the case of $^{14}\text{N}_2\text{O}$, the $\nu_3 = 1 \leftarrow 0$, P(18) and $\nu_3 = 2 \leftarrow 1$, R(17) transition frequencies (where ν_3 is the anti-symmetric stretching mode) differ by 6.8 GHz.^{13,14} This means that the overall, $2 \leftarrow 0$, Q(18) two-photon transition, which is observed in Ref. [12], has a relatively small one-photon detuning of $\frac{6.8}{2}$ GHz. In comparison, for 1C2P detection of $^{13}\text{CO}_2$, the smallest one-photon detuning is nearly $\frac{42}{2}$ GHz (for the $1 - 0$, P(16) and $2 - 1$, R(15) pair).¹³ Given that the 1C2P excitation probability is proportional to the inverse of the *square* of the one-photon detuning, the detection sensitivity of $^{13}\text{CO}_2$ will likely be more than an order of magnitude lower than that of $^{14}\text{N}_2\text{O}$. We must point out that variations in the 1C2P detection sensitivity are expected to be reduced for detection of heavy asymmetric top molecules, due to their more complex and dense energy level structures.¹⁰ For these larger asymmetric top species, 1C2P transitions with one-photon detunings less than the Doppler width could typically be expected.¹⁰ Nevertheless, the reliance on the presence of small one-photon detunings is a key limiting factor for the general application of the

1C2P-CRD technique, especially for detection of small molecules.

In light of the need for a generalized detection scheme with both high sensitivity and selectivity, we present in this work a proof of principle demonstration of two-color, intra-cavity pump-probe CRD detection of $^{14}\text{N}_2\text{O}$ in a three-mirror, traveling-wave cavity (the isotope mass label on N will be dropped from here on). The N_2O molecule is chosen for

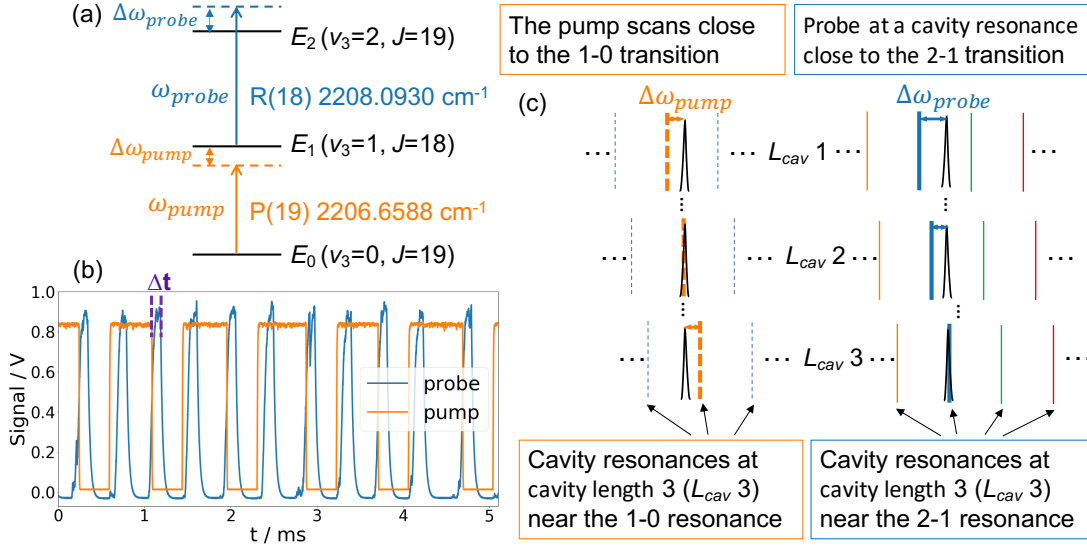


FIG. 1: Experimental schemes. (a) Diagram that illustrates the interaction of a three-level-system with two laser radiation sources. The rotation-vibration assignments for the three levels of interest are given in the parentheses.^{13,14} E_i is the energy of level i ($i = 0, 1, 2$). ω_{pump} and ω_{probe} are the angular frequencies of the pump and probe lasers. $\Delta\omega_{pump}$ and $\Delta\omega_{probe}$ are, respectively, the pump and probe detuning frequencies from the corresponding molecular transition frequencies (see Eqs. 2 for the exact definitions). (b) The time traces of the pump and probe signals, obtained with the 1:1 pump switching scheme. Δt gives the delay between the pump shut-off time and the start of the probe ringdown (see Section II). (c) Basic principles of our pump and probe frequency scanning scheme. The vertical lines represent selected cavity resonances at three different cavity lengths (L_{cav}). Three cavity resonances (dashed lines) are shown near the 1 – 0 transition frequency, and four (solid lines) near the 2 – 1 transition frequency. For illustration purposes, the pump and probe lasers in (c) are frequency-locked, respectively, to cavity resonances indicated by the thick orange and blue bars. A decrease in the cavity length leads to a *simultaneous* increase in both the pump and probe frequencies (i.e. the vertical bars move to the right as L_{cav} decreases from 1 to 3).

our demonstration, because the frequencies of a pair of linked ro-vibrational transitions of N₂O (Fig. 1a), $\nu_3 = 1 \leftarrow 0$, P(19) (pump) and $\nu_3 = 2 \leftarrow 1$, R(18) (probe), are within the frequency tuning ranges of the available QCLs at our laboratory. Both transitions have been experimentally measured.^{13,14} Based on the $\nu_3 = 2 \leftarrow 1$ (*ab initio*)¹⁵ and $\nu_3 = 1 \leftarrow 0$ (experiments)¹⁶ transition frequencies of ¹⁴CO₂, two-color pump-probe detection of ¹⁴CO₂ is currently not possible at our laboratory, due to the limited frequency tuning ranges (~ 6 cm⁻¹) of the available QCLs. The natural scarcity of ¹⁴CO₂ and the uncertainties for its $\nu_3 = 2 \leftarrow 1$ transition frequencies (none of which has been experimentally observed) add to the experimental complexities of two-color detection of ¹⁴CO₂. For these reasons, we believe that the N₂O molecule is a more suitable candidate for the initial demonstration of the two-color CRD technique. Experimental demonstration of two-color detection of ¹⁴CO₂ will be conducted in the near future.

The basic principles of our two-color experiment on N₂O are illustrated in Fig. 1. The counter-propagating pump and probe lasers are each frequency-locked, respectively, to a cavity resonance close to the $\nu_3 = 1 \leftarrow 0$, P(19) and $\nu_3 = 2 \leftarrow 1$, R(18) molecular transition frequencies (see Figs. 1a and 1c). Our simulation model (Section III) is used to determine which specific pairs of pump-probe cavity resonances are used to observe two-color CRD signals. In our experiment, the intracavity pump radiation (estimated to be 36 W without attenuation) is switched off during every other probe ringdown event (Fig. 1b). The difference between the pump-on and pump-off signals yields the net N₂O two-color absorption. Since the pump-off signal contains information of both the empty-cavity ringdown rates and the overlapping background one-photon absorption from non-target molecular species, the net two-color CRD signals are, in principle, free of these two types of background interference. Unlike the *free-space*, two-color excitation, for the *intracavity* two-color excitation, the pump and probe laser frequencies are each only allowed at a specific cavity resonance (see Fig. 1c). Due to the constraint of the cavity resonance conditions on the laser frequencies, the probe laser frequency cannot be tuned independently of the pump, because a change in the cavity free-spectral-range (\mathcal{FSR}) leads to a *simultaneous* shift in both the pump and probe frequencies (Fig. 1c).

To our knowledge, two-color excitation has not been widely applied with cavity-enhanced techniques, despite the routine application of its free-space version in spectroscopy for enhancing detection selectivity in the presence of spectral congestion. We are only aware

of two recent works which reported the use of two-color CRD detection.^{17,18} The pump-probe schemes applied in those works differ substantially from ours, which utilizes a pair of strong, $\Delta v = 1$, mid-IR ro-vibrational transitions. The pump transition in our two-color detection is strongly power-broadened (FWHM \sim 1 GHz), as a result of the cavity-enhanced pump radiation power (36 W) (see discussions in Section IV A and Appendix A). The entire Doppler-profile of the pump transition can be efficiently excited with nearly equal probabilities, even at relatively large pump detuning frequencies (\pm 1 GHz). In the work reported in Ref. [17], the pump laser (3000 nm) excites the ν_3 -fundamental transition of acetylene, and a second laser (1550 nm) is used to probe the $\nu_1 + 2\nu_3 \leftarrow \nu_3$ transition. Given that the cavity mirrors (with optimized reflectivity in the near-IR) are transmissive in the mid-IR region, the mid-IR pump (100 mW) undergoes a single-pass through the cavity. The pump power is not cavity-enhanced. In addition, the near-IR probe can be tuned independently from the pump laser, the frequency of which is fixed on the acetylene ν_3 -fundamental transition frequency. The experiments reported in Ref. [18] are similar to ours in that the pump and probe lasers (1.6 μ m) are simultaneously coupled into a high-finesse ($F \sim 100000$) cavity. However, both the pump and probe near-IR transitions used in Ref. [18] are weak overtone-combination band ($\Delta v_1 = +3$, $\Delta v_3 = +1$) transitions of CO₂, with transition dipole moments more than 20 \times weaker than the N₂O ro-vibrational transitions used in our experiments. Due to the use of weak pump transitions in Ref. [18], the two-color CRD signals are only observed when the frequencies of the counter-propagating pump and probe lasers are both on resonance for a particular velocity group of CO₂. In contrast to this Doppler-hole-burning-type two-color detection of Ref. [18], strong two-color signals are observed in our experiments at pump detuning frequencies ($>$ 600 MHz) well outside the Doppler FWHM (120 MHz) of the N₂O, $\nu_3 = 1 \leftarrow 0$, P(19) transition, due to the strong power broadening of this pump transition.

We believe that our intracavity, ladder-type pump-probe scheme, which utilizes strong mid-IR 1 – 0 (pump) and 2 – 1 (probe) ro-vibrational transitions, is ideal for high-sensitivity and high-selectivity trace-gas detection. As far as we are aware, two-color, cavity-enhanced detection schemes similar to ours have not been reported in the literature. Given that the 1 – 0 and 2 – 1 ro-vibrational transitions typically have similar transition frequencies, both the pump and probe radiation can be cavity-enhanced. With the high intracavity pump power (36 W) that can be achieved in our setup, the fundamental-band transition (\sim 0.1 Debye transition dipole) is easily saturated at the pressure conditions typical for mid-IR,

CRD measurements (20–30 torr). At the same time, the detection sensitivity is greatly enhanced because of the long effective absorption pathlength for the probe (7.1 km). Due to the presence of strong intracavity pump radiation, effects from strong light-molecule interactions, such as power broadening and light shifts, become important in our pump-probe scheme. These effects are treated in this work by the three-level system density-matrix formalism, which is solved under the cavity resonance constraints (Section III). Our model further suggests that, with a strongly saturated pump transition, the two-color signals based on our pump-probe scheme should be essentially as strong as the signals from conventional, one-color detection of the mid-IR, fundamental-band transitions. Even though the pump can only excite maximally half of the population into the intermediate level, this “loss” in the population is largely compensated by the fact that the $2-1$ probe transition probabilities are typically higher than those of the $1-0$ transition (by a factor of two in the harmonic oscillator limit).¹⁰ For both N_2O and CO_2 , for example, the transition probabilities of $\nu_3 = 2 - 1$ are close to $1.9\times$ larger than those of $\nu_3 = 1 - 0$.¹³

We must point out that, while room-temperature, CRD-detection-based quantification of $^{14}\text{CO}_2$ samples at concentrations below the ^{14}C natural abundance is the original motivation for the development of our two-color CRD detection, the potential use of our technique is not limited to trace-detection of small molecules. With the development of widely tunable and high power mid-IR radiation sources, our intracavity pump-probe detection can be applied for quantum-state-resolved, spectroscopic studies of vibrationally excited states of large and non-volatile molecular species, for which experimental challenges due to spectral congestion and low gas-phase density call for the use of high sensitivity and high selectivity detection methods.¹⁹

II. EXPERIMENTAL DETAILS

A schematic of our experimental setup is shown in Fig. 2. The three-mirror, traveling-wave cavity, with total nominal round trip length of 66 cm, consists of two plano mirrors and a plano-concave mirror with 1-m radius of curvature (LohnStar). The two plano mirrors are glued directly onto an invar cavity spacer. The concave mirror is housed in a piezoelectric transducer (PZT) assembly which is attached to the invar spacer. The laser incidence angle at the PZT mirror is $\sim 1.5^\circ$. Two continuous-wave (cw) distributed feedback quantum

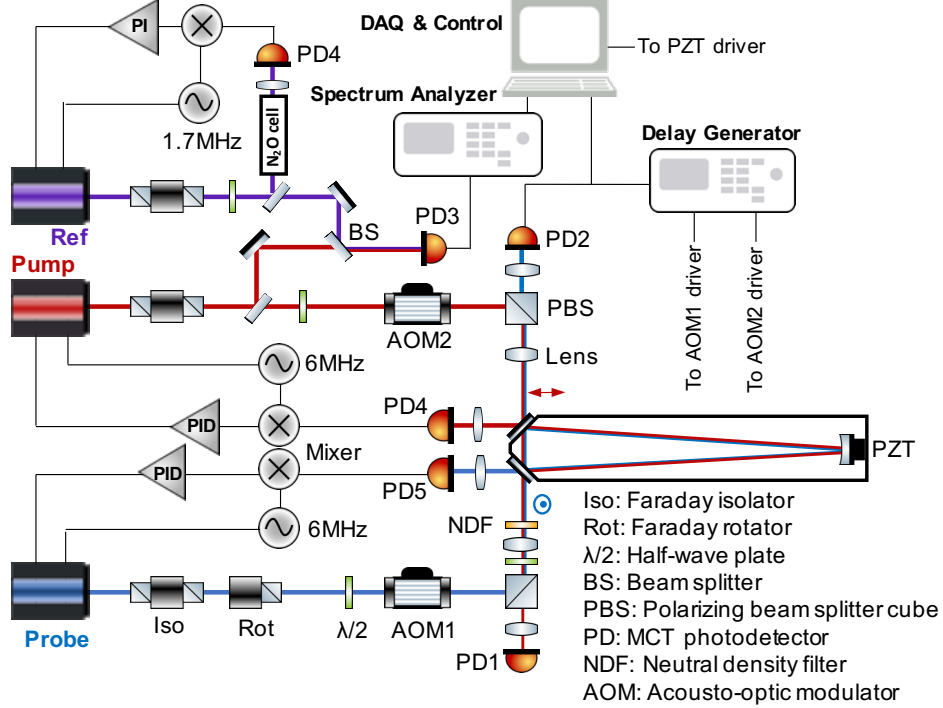


FIG. 2: The experimental setup. The three QCLs are labeled as “Pump”, “Probe”, and “Ref”. The counter-propagating Pump and Probe are coupled into the ring-cavity for the two-color CRD measurements, and their respective polarizations are indicated by the standard arrow-dot symbols. The Ref laser, which is frequency-locked to the N_2O 1–0, P(19) transition, serves as the frequency reference of our experiment. See text for more details about the experimental setup.

cascade lasers (QCL) (Hamamatsu HHL-package), labeled as “Pump” and “Probe” in Fig. 2, are coupled into the traveling-wave cavity in a counter-propagating configuration. The pump laser is p -polarized, and the probe s -polarized with respect to the cavity. Since the two plano cavity mirrors have higher reflectivity for s - vs. p -polarization, the cavity has a higher finesse for the probe than the pump. The s -mode probe ringdown time is measured to be $23.7 \mu\text{s}$ (with finesse of $F = 67700$), and the p -mode pump ringdown time is $1.85 \mu\text{s}$ ($F = 5280$). With two polarizing beam splitter cubes (Electro-Optics Technology, 1000 : 1 extinction ratio), the two counter-propagating, orthogonally-polarized laser beams can be easily separated and individually detected. Both pump and probe QCLs are frequency-locked to the cavity by the Pound-Drever-Hall (PDH) method.²⁰ Specifically, for each laser (modulated at 6 MHz), light reflection off the cavity is measured with a HgCdTe (MCT) photodetector (PD4/PD5 in Fig. 2, Thorlabs PDAVJ8), and the MCT signal is demodulated

with a frequency mixer (Mini-Circuit, ZRPD-1+). The resulting error signal is used as the input to the PID servo control loop (Vescent D2-125-PL) to achieve laser frequency-locking to the cavity.

The probe laser beam is detected by another MCT photodetector (PD2 in Fig. 2, VIGO PVI-3TE-6/MIPDC-F-20). A small portion of the MCT output is sent to a delay generator (Stanford Research System DG645), which sends a trigger to AOM1 (IntraAction) to initiate the probe ringdown when the MCT signal reaches a preset threshold. The remaining MCT signal is digitized on a 24-bit oscilloscope (National Instrument PXI-5922). To measure the background cavity ringdown rates, the intracavity pump power is switched off after every other probe ringdown event. This 1:1 pump switching sequence is achieved with a separate output channel of the delay generator to control AOM2 (IntraAction). The delay between the pump shut-off and the start of the probe ringdown can be varied. Figure 1b shows both the pump and probe signals, where a 250- μ s-long signal is recorded for each probe ringdown event and a pump-probe delay (Δt) of 100 μ s is used. As can be seen in Fig. 1b, we are able to achieve sustained intracavity pump power, with $\sim 0.5\%$ intensity fluctuation. A sustained and stable intracavity pump power is crucial for the success of our two-color detection scheme. A large pump-probe delay ($\Delta t > 100 \mu$ s) is needed, especially at low pressure (2.6 torr), to avoid exciting (small) residual populations in the pump-populated $v_3 = 1, J = 18$ level after the intracavity pump power is shut off by AOM2 (see Appendix A for more details). By using a 250- μ s ringdown data collection window and $\Delta t = 100 \mu$ s, we achieve probe ringdown acquisition rates of ~ 2 kHz in our setup. The difference between the ‘‘Pump-on’’ and ‘‘Pump-off’’ signals yields the background-free, two-color N₂O signal. As illustrated in Fig. 1c, the pump and probe lasers are frequency-locked to a specific cavity resonance close to, respectively, the 1–0 and 2–1 molecular transition frequencies. The two laser frequencies are simultaneously tuned by changing the cavity \mathcal{FSR} , which is achieved by adjusting the PZT voltage. For all of the spectra in this work, at each PZT position, 1-s of ringdown events are recorded and analyzed.

To minimize power saturation of the probe transitions while maintaining near-maximum signal at the detector, the *s*-mode laser beam is attenuated with neutral density filters (with total OD=1.2) prior to being coupled into the cavity. However, even with this attenuated probe laser beam, we still observe clear signs of power saturation in the ringdown traces (i.e. non-exponential decay), particularly at the early part of the ringdown signals at low

pressure (2.6 torr). To further minimize saturation at low pressure, the starting point of our exponential ringdown fit is chosen to be $50 \mu\text{s}$ ($\sim 2 \times$ ringdown-time) later than the start of probe ringdown. The intracavity *s*-mode power is estimated to be equivalence of 0.2 W at the beginning of the fit of the exponential ringdown. The cw intracavity *p*-mode power is ~ 36 W.

In our current setup, the cavity is mounted on a typical optical table, without active compensation of ambient perturbations (e.g. acoustics, temperature, pressure). Due to the presence of a small gas leak in the cavity mirror epoxy (~ 1 mtorr/min), all our measurements are taken under the gas flow-through condition, which does not noticeably degrade the laser locking performances. The successful implementation of two-color CRD measurements under these noisy experimental conditions demonstrates the potential of our technique for future field-work applications. In our setup, the cavity pressure is controlled with a needle valve located near the gas inlet of the cavity, which is evacuated by a turbo pump. Ultra high-purity N_2 is used for all the measurements. In our flow-through setup, the N_2O concentration derives from the established equilibrium between the flow-through cavity and the ambient air (~ 330 ppb N_2O). The N_2O concentration (down to 0.1 ppb level) inside the cavity can be varied by adjusting a combination of the needle-valve opening, the head pressure at the valve, and the pump rate. The N_2O concentration used for a given two-color CRD measurement is determined by directly measuring the one-photon CRD signal of the $1 - 0$, P(17) transition at $2208.5751 \text{ cm}^{-1}$.^{13,14} The one-photon CRD signal is fitted using both the conventional exponential decay fit (to the late-gated signal) and the SCAR method (with fixed value for the initial saturation parameter, following the procedures in Refs. [5,6]). The average value of the N_2O concentration determined from these two fitting methods and their difference (taken as the measurement error) are both reported in this work.

The experimental components associated with the third laser (labeled as “Ref” in Fig. 2) are used for the calibration of the pump and probe laser frequencies. Specifically, this third QCL (Hamamatsu HHL-package) is frequency-modulated at 1.7 MHz, and passes through a static cell with 7.2 torr of 0.01% N_2O in N_2 . The Ref laser is locked to the N_2O $1 - 0$, P(19) transition by a PI servo loop (New Focus LB1005). As the pump laser frequency is scanned in the vicinity (± 0.85 GHz) of the same N_2O $1 - 0$ transition, the beatnote between Pump and Ref QCLs provides a sufficiently accurate (± 0.5 MHz with 1-s averaging) pump detuning frequency measurement ($\Delta\omega_{10}$). The beatnote signal is measured by a fast MCT

detector (VIGO) and recorded on a spectrum analyzer (Rhode & Schwartz). The pump laser frequency can be determined from the measured pump detuning value and the N₂O 1 – 0, P(19) transition frequency.^{13,14} The calibration of the probe laser frequency requires additional measurements of cavity properties, such as the cavity \mathcal{FSR} (discussed below).

For an ideal three-mirror ring-cavity, for which all three incidence angles for the intracavity radiation are smaller than the Brewster angle, a given cavity p -mode resonance is located half-way between the two closest s -mode resonances, because of the net π phase-shift difference between the two polarizations upon mirror reflections at non-normal incidence angles.²¹ In comparison, the two polarization modes are degenerate in a linear, Fabry-Perot cavity. Furthermore, as a result of small differential phase shifts between s - and p -polarized light upon interaction with the mirror coatings, the p -mode resonance frequencies in a typical ring-cavity do not lie exactly mid-way from the two neighboring s -mode resonance frequencies.²¹ For our purpose, we define this displacement, $\delta\nu_{sps}$, to be the difference of the p -resonance frequency from the average frequency of two adjacent s -resonances. From the beatnote measurements between multiple pairs of PDH-locked p - and s -mode transmitted light with frequency difference <2 GHz, both the cavity \mathcal{FSR} and $\delta\nu_{sps}$ values can be determined with sub-kHz accuracy. At zero PZT voltage, $\mathcal{FSR}=443.3686$ MHz, and $\delta\nu_{sps}=+32.5954$ MHz (measured at 2209.5 cm^{-1}). Together with the ω_{pump} value derived from the pump detuning measurement, the probe laser frequency can be determined by

$$\omega_{probe}/2\pi = (\omega_{pump}/2\pi - \delta\nu_{sps} + \mathcal{FSR}/2) + n\mathcal{FSR} \quad (1)$$

where n is an integer. With the probe laser frequency measurement provided by the wavemeter (Bristol 771) (10 MHz accuracy), n can be determined unambiguously ($n = 97 - 99$ for our pump-probe scheme). With this probe laser frequency and the $2 - 1$, R(18) transition frequency from HITRAN,^{13,14} the probe detuning frequency can be determined to the accuracy of the HITRAN values (~ 10 MHz). Small change in the \mathcal{FSR} value ($\Delta\mathcal{FSR} < 7$ kHz) during a 0.85 GHz pump/probe frequency scan is neglected in calculating the probe laser frequency, since the error introduced by this simplification ($n\Delta\mathcal{FSR}$) is significantly smaller than the expected probe frequency calibration error (~ 10 MHz). We note that the pump and probe laser frequency calibration procedures could be greatly simplified in the future with the use of a mid-IR frequency comb as a frequency reference.

III. SIMULATION MODEL

For the three-level system considered in this work (Fig. 1a), the $1-0$ and $2-1$ transition frequencies differ by $\sim 1.5 \text{ cm}^{-1}$ (45 GHz). Given that each laser is in near-resonance with only one of the two transitions, the effects of cross-excitation, e.g., the pump exciting the $2-1$ transition, are neglected. With the one-photon pump and probe detunings defined, respectively, as

$$\begin{aligned}\Delta\omega_{pump} &= \omega_{pump} - (E_1 - E_0)/\hbar + \Delta\omega_{pump}^{\text{Doppler}} \\ \Delta\omega_{probe} &= \omega_{probe} - (E_2 - E_1)/\hbar + \Delta\omega_{probe}^{\text{Doppler}},\end{aligned}\tag{2}$$

where $\Delta\omega_{pump}^{\text{Doppler}}$ and $\Delta\omega_{probe}^{\text{Doppler}}$ are the Doppler-induced pump and probe detunings for a given velocity sub-group, the time-evolution of the density matrix elements (under the rotating-wave approximation) are given by the following system of differential equations,

$$\begin{aligned}-\dot{\rho}_0 &= \gamma_0(\rho_0 - 1) + i\Omega_{10}(\rho_{01} - \rho_{10}) \\ -\dot{\rho}_1 &= \gamma_1\rho_1 + i\Omega_{10}(\rho_{10} - \rho_{01}) + i\Omega_{21}(\rho_{12} - \rho_{21}) \\ -\dot{\rho}_2 &= \gamma_2\rho_2 + i\Omega_{21}(\rho_{21} - \rho_{12}) \\ -\dot{\rho}_{01} &= i\Omega_{10}(\rho_0 - \rho_1) + (\gamma_{10} + i\Delta\omega_{pump})\rho_{01} + i\Omega_{21}\rho_{02} \\ -\dot{\rho}_{20} &= i\Omega_{21}\rho_{01} + [\gamma_{20} + i(\Delta\omega_{pump} + \Delta\omega_{probe})]\rho_{02} - i\Omega_{10}\rho_{12} \\ -\dot{\rho}_{12} &= i\Omega_{21}(\rho_1 - \rho_2) + (\gamma_{21} + i\Delta\omega_{probe})\rho_{12} + i\Omega_{20}\rho_{20} \\ \rho_{01} &= \rho_{10}^*, \quad \rho_{20} = \rho_{02}^*, \quad \rho_{12} = \rho_{21}^*,\end{aligned}\tag{3}$$

where ρ_i gives the population in level i ($i = 0, 1, 2$) and ρ_{ij} gives the coherence between level i and j . Furthermore, E gives the electric field amplitude at the position of the molecule; $\Omega_{10} = \mu_{10}E/2\hbar$ and $\Omega_{21} = \mu_{21}E/2\hbar$ are, respectively, half of the Rabi-frequency of the $1-0$ and $2-1$ transition, with corresponding electric transition dipole moment, μ_{10} and μ_{21} ; γ_i is the population decay rate for level i , and γ_{ij} is the coherence decay rate between level i and j . Note that the pump and probe detuning frequencies given by Eqs. 2 are the *negative* values of how these two detunings are typically defined in the literature, e.g., the one-photon pump detuning (without the Doppler contribution) is conventionally defined as $(E_1 - E_0)/\hbar - \omega_{pump}$. With our alternative definitions, the pump/probe detuning value increases as the laser frequency increases, which is natural when the spectrum is shown as a function of these detunings. A positive/negative detuning now corresponds to blue/red

detuning. Given that the cavity-decay time (23.7 μs) is much longer than the collisionally-induced dephasing time (~ 100 ns at 1 torr, the lowest pressure used in our experiment), the system is assumed to have reached and remain in the steady state throughout the probe ringdown. As a result, the time-derivatives on the left-hand-side of Eqs. 3, $\dot{\rho}_i$ and $\dot{\rho}_{ij}$, are set to zero. The two-color excitation signals are taken to be proportional to $\gamma_2\rho_2$, which is the steady-state photon absorption rate into level 2 by the probe laser.¹⁰

With the constraints on the pump and probe frequencies given by Eq. 1, the two-color excitation spectra for a given set of $1 - 0$ and $2 - 1$ molecular transitions are simulated by solving Eqs. 3 with an array of cavity \mathcal{FSR} values. A change in the \mathcal{FSR} values leads to a simultaneous scan in the pump and probe radiation frequencies (by approximately $4 \times \mathcal{FSR}$ in our simulation). The smallest \mathcal{FSR} value in our simulation is set to the measured \mathcal{FSR} at zero PZT voltage, which is typically the starting voltage of an experimental frequency scan. The p -mode displacement parameter, $\delta\nu_{sps}$, which has also been measured at zero PZT voltage, is assumed to increase proportionally to \mathcal{FSR} , i.e., $\delta\nu_{sps}/\mathcal{FSR}$ is a constant. In our simulation, the pump radiation is set to follow a p -mode cavity resonance with frequency detunings in the range of ± 850 MHz from the $1 - 0$ transition frequency. Our simulation shows that, regardless of the pump-probe transition frequencies, the two-color excitation signals can be observed at some pump detunings if the probe signals are recorded for one of the s -mode cavity resonances with an initial probe frequency detuning in the range of approximately $\pm \mathcal{FSR}$ at the beginning of the frequency scan.

To take into account the Doppler-broadening effects (FWHM=120 MHz at 300 K for N_2O), at each \mathcal{FSR} value, the ρ_2 values for various Doppler velocity sub-groups are numerically integrated. In our simulation, 200 sub-groups spanning ± 250 MHz of Doppler detunings are included. The Doppler effects produce different combinations of pump and probe detunings for each of the velocity sub-groups. For each sub-group, $\Delta\omega_{pump}^{\text{Doppler}} + \Delta\omega_{probe}^{\text{Doppler}} \approx 0$, because of the closeness of the pump and probe laser frequencies and the counter-propagating beam configurations. This (near-)perfect Doppler cancellation is the basis for the observation of Doppler-free, two-photon transitions in our two-color experiments. With the use of a strong pump, we observe, in addition to these narrow Doppler-free transitions, Doppler-broadened two-color transitions (see Section IV).

In our simulations, the air-broadening coefficients for N_2O (HWHM=3 MHz/torr for both $2 - 1$ and $1 - 0$)^{13,14} are used to calculate γ_{10} , γ_{21} , and γ_{20} . A probe half-Rabi-frequency

of $\frac{\Omega_{21}}{2\pi} = 1$ MHz is used in our simulation to allow for probe power saturation. The pump half-Rabi-frequency, Ω_{10} , and the population decay rate, γ (which is assumed to be the same for all three levels), are adjusted to match the observed two-color spectra. Note that each of the three levels involved in our excitation scheme has $(2J + 1)$ -fold degeneracy, due to the presence of magnetic sub-levels (m sub-levels). The transition dipole moments are m -dependent. Technically, the two-color spectra should be calculated for each of the m sub-levels involved in the transition scheme. However, we find that calculations which explicitly take into account m -dependent transition dipole moments are not necessary to reproduce key spectroscopic features observed in the two-color spectra. For simplicity, a single effective value is used for each of the Ω_{10} and Ω_{21} parameters. Effects on the Rabi-frequencies from the Gaussian radial beam profile and variations of the beam radius along the cavity longitudinal direction are also incorporated into these effective Ω_{10} and Ω_{21} values. The intensities of the simulated two-color spectra are scaled using the predicted signal intensity ratios of the two-color and the $1 - 0$, one-color transitions (simulated with the same probe laser power), and the experimentally measured $1 - 0$, P(17) transition peak intensities.

To summarize, the following set of values are used in our simulation of the observed N_2O two-color spectra: $\gamma_{10}/P = \gamma_{21}/P = \gamma_{20}/P = 2\pi \times 3$ MHz (where P is the pressure in torr), $\gamma/P = 2\pi \times 30$ kHz, $\Omega_{10} = 2\pi \times 25$ MHz, and $\Omega_{21} = 2\pi \times 1$ MHz. As discussed in Appendix A, to reproduce key spectroscopic features observed in the two-color CRD spectra (in particular, the relative intensities between the Doppler-free and Doppler-broadened peaks), our simulation model requires the population decay rates to be significantly slower than the coherence decay rates. For a given ro-vibrational transition, these two types of collision-induced rates are generally similar.^{22,23} Collisions which are strong enough to interrupt the coherence between two ro-vibrational levels are expected to lead to changes in both the m (because the m sub-levels are degenerate for a given J level) and J quantum number (because the rotational energy spacings are small compared to the thermal energy at room temperature, $k_B T \sim 200$ cm⁻¹).²² We believe that the unusually slow population decay rates inferred from our simulation is an artifact of the phenomenological treatment of collisional relaxations by Eqs. 3, discussed in Appendix A. We emphasize that the simulation model described in this section provides accurate predictions of the pump and probe frequencies for observing two-color resonances in a cavity. In addition, it provides physical insights into the appearance of the observed two-color spectra. More exact treatments of the collisional pro-

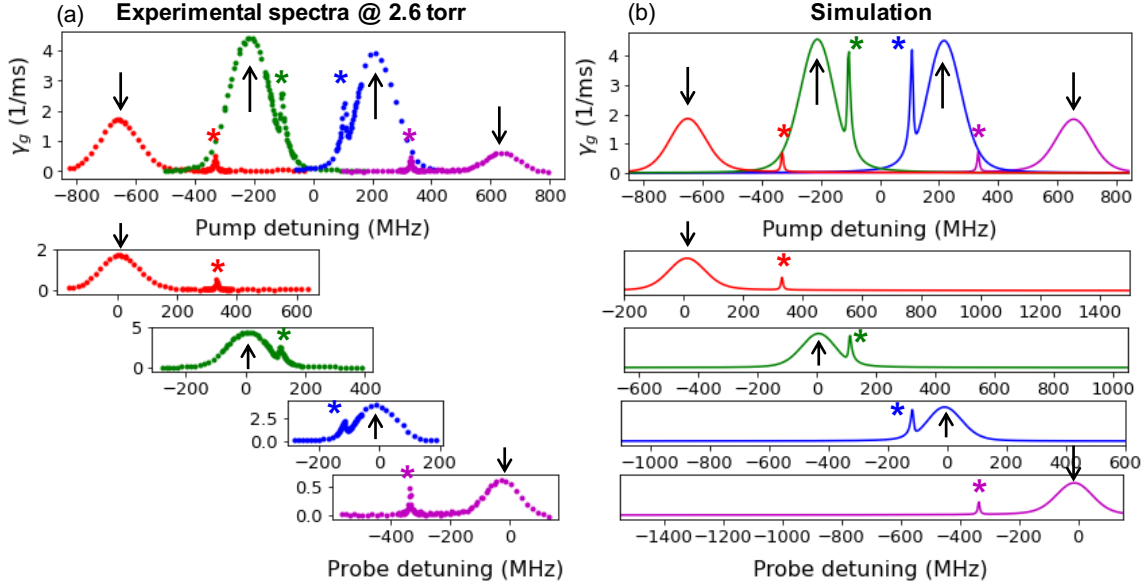


FIG. 3: Experimental (a) and Simulated (b) two-color CRD spectra recorded at 2.6 torr. The two upper panels in (a) and (b) show four overlaid, two-color spectra as a function of the pump detunings. Each of the four lower panels shows the individual two-color spectrum as a function of the probe detunings. The N_2O concentration is 32.3 ± 0.1 ppb. The asterisks and arrows (both upward and downward) are used to indicate, respectively, the coherent two-quantum resonances and stepwise two-color resonances, which are discussed in detail in Section IV A. Note that the relative intensities between the two stepwise resonance peaks indicated by the downward-pointing arrows in (a) are not reproduced by our simulations in (b). The origin of this observed asymmetry is discussed in Section IV A and the Supplemental Information.

cesses as well as the effects from m sub-levels and the radiation intensity profiles are needed to quantitatively reproduce the intensity patterns of the observed two-color spectra, which is not achieved with our basic model (including its five-level-system extension, discussed in the Supplemental Information).

IV. RESULTS AND DISCUSSIONS

A. Spectroscopic features in the two-color spectra

According to the simulation based on our pump-probe scheme (Fig. 1a), with pump detunings in the range of ± 0.85 GHz, two-color pump-probe signals can be observed in four

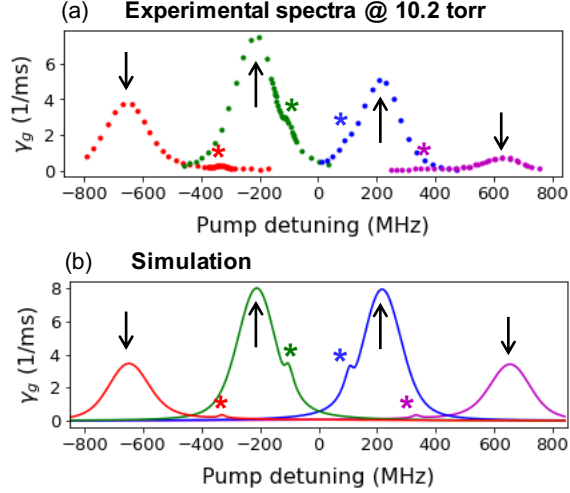


FIG. 4: Experimental (a) and Simulated (b) two-color CRD spectra taken at 10.2 torr. Four two-color spectra are overlaid and shown together as a function of the pump detunings. The N_2O concentration is 12.4 ± 0.8 ppb. As in Fig. 3, the asterisks and arrows (both upward and downward) are used to indicate, respectively, the coherent two-quantum resonances and the stepwise two-color resonances.

separate frequency scans in which the pump and probe lasers are frequency-locked to four different pairs of p - and s -mode cavity resonances with frequencies close to the corresponding target molecular transitions (see the illustrations in Fig. 1c, in which the pump and probe are locked to one such pair of p - and s -mode cavity resonances). These four two-color spectra are shown in Figs. 3a and 4a for measurements made at 2.6 and 10.2 torr, respectively. The numerically simulated spectra at these two pressures are shown in Figs. 3b and 4b. For both sets of experimental spectra, the signals correspond to the background-free, two-color, N_2O -induced absorption rate (γ_g). In the two upper panels of Fig. 3 (experiment and simulation at 2.6 torr), the four two-color spectra are overlaid and shown together as a function of the pump detunings. In the bottom four panels, these four spectra are shown individually as a function of the probe detunings. In Fig. 4 (for experiments at 10.2 torr), the overlaid, pump-detuning spectra are shown. Each two-color peak in Fig. 4 occurs at the same probe detuning frequency as its corresponding peak in Fig. 3, e.g., the peaks indicated by the arrows in Figs. 3a and 4a all occur at close to zero probe detuning. To avoid redundancy, the probe-detuning spectra at 10.2 torr are not shown in Fig. 4. We emphasize that the observed two-color signals in Figs. 3a and 4a all arise from a single pump-probe scheme

(Fig. 1a). The presence of two-color peaks in multiple frequency scans is a consequence of the *intracavity* pump-probe excitation, for which the cavity-constraint pump and probe laser frequencies are simultaneously changed, i.e., the pump laser frequency cannot be set at a fixed value as in conventional, *free-space*, pump-probe experiments.

There are two qualitatively different types of two-color resonances observed in our experiment, as can be seen more clearly in the low-pressure spectra (Fig. 3). The narrow, Doppler-free, two-color resonances (four such resonances with FWHM of ~ 15 MHz are indicated by the asterisks in Fig. 3) occur at pump and probe detunings that are equal in magnitude (subject to AC Stark shift of ~ 1 MHz) but opposite in sign. As explained in Section III, these sharp, Doppler-free resonances occur due to the counter-propagating pump-probe configuration. The intermediate $\nu_3 = 1$ level is *not* populated during this coherent excitation scheme, i.e., a Raman-type process which exploits a virtual intermediate state. Note that, due to pressure broadening, the Doppler-free peaks (indicated by the asterisks in Fig. 4) show up only weakly at 10.2 torr. In addition to these Doppler-free two-color resonances, we observe strong Doppler-broadened features in our two-color spectra (indicated by the arrows in Figs. 3 and 4). These broad features always occur at nearly zero probe detuning. According to our simulation, these Doppler-broadened features result from a two-step excitation, $2 \leftarrow 1 \leftarrow 0$. The intermediate $\nu_3 = 1$ level is first *physically* populated by the pump laser at some detuning value. At that particular detuning, if the probe laser frequency (constrained by Eq. 1) is close to the $2 - 1$ resonance frequency (e.g. within the $2 - 1$ Doppler FWHM), the $2 \leftarrow 1$ excitation then occurs. Note that the two peaks indicated by the downward-pointing arrows in Fig. 3a occur, respectively, at pump detunings of -655 MHz and $+635$ MHz, both of which are well outside the $1 - 0$ Doppler FWHM (120 MHz). As a result, the intermediate $\nu_3 = 1$ level must be populated through strong power-broadening of the $1 - 0$ transition, with a power-broadened linewidth of ~ 1 GHz. Since all the Doppler velocity sub-groups are simultaneously populated by the strong pump with nearly equal probabilities at all pump-detunings, the Doppler compensation that occurs for the two-photon, Raman-type excitation no longer applies for the $2 \leftarrow 1 \leftarrow 0$ two-step excitation. In the following discussions, the narrow two-photon peaks are referred to as the coherent two-quantum resonances, and the Doppler-broadened two-photon peaks as stepwise resonances.

As discussed in Appendix A, the large power-broadened linewidth (FWHM ~ 1 GHz) and

strong power-saturation of the $1 - 0$ transition result from a combination of moderately high pump Rabi-frequency and the long collision-induced vibrational relaxation time for the $\nu_3 = 1$ vibrational state ($21 \mu\text{s}$ for collisions with N_2 at 10 torr).^{24,25} In the presence of the pump radiation, the long vibrational relaxation time leads to a slow *net* population decay rate from the pump-populated $\nu_3 = 1$, $J = 18$ level. The degree of saturation for the $1 - 0$ transition and its power-broadened width are both enhanced due to this slow population decay. Similarly long vibrational relaxation time has been reported for the $\nu_3 = 1$ level of $^{12}\text{CO}_2$ ($6 \mu\text{s}$ for collisions with N_2 at 10 torr).²⁶

As can be seen in Figs. 3a and 4a, the four coherent, two-quantum peaks occur at pump detunings close to $-\frac{3}{4}\mathcal{FSR}$, $-\frac{1}{4}\mathcal{FSR}$, $\frac{1}{4}\mathcal{FSR}$, $\frac{3}{4}\mathcal{FSR}$, and the stepwise peaks at detunings close to $-\frac{3}{2}\mathcal{FSR}$, $-\frac{1}{2}\mathcal{FSR}$, $\frac{1}{2}\mathcal{FSR}$, $\frac{3}{2}\mathcal{FSR}$. This near-symmetry in the peak frequency values with respect to zero pump detuning is a consequence of a fortuitous situation where the difference between the N_2O , $1 - 0$, P(19) and $2 - 1$, R(18) transition frequencies ($\Delta\nu$) is close to an exact integer multiple ($97\times$) of the cavity \mathcal{FSR} value. Given the frequency difference between the pump (p -mode) and probe (s -mode) cavity resonances (Eq. 1), the stepwise two-color resonances are expected to occur at pump ($\Delta\nu_{pump}^{sw}$) and probe ($\Delta\nu_{probe}^{sw}$) detunings close to (neglecting the pump-induced light shifts)

$$\begin{aligned}\Delta\nu_{probe}^{sw} &\approx 0, \\ \Delta\nu_{pump}^{sw} &\approx \Delta\nu - [(n + 1/2)\mathcal{FSR} - \delta\nu_{sps}],\end{aligned}\tag{4}$$

where the approximate relationship for $\Delta\nu_{pump}^{sw}$ is derived as a result of the first condition, $\Delta\nu_{probe}^{sw} \approx 0$ (see the discussion in the preceding paragraph). Similarly, considering that $\Delta\nu_{probe}^{2q} + \Delta\nu_{pump}^{2q} \approx 0$ for the coherent, two-quantum peaks, these Doppler-free resonances are expected at pump ($\Delta\nu_{pump}^{2q}$) and probe ($\Delta\nu_{probe}^{2q}$) detunings values

$$\begin{aligned}\Delta\nu_{pump}^{2q} &\approx \frac{1}{2} \{ \Delta\nu - [(n + 1/2)\mathcal{FSR} - \delta\nu_{sps}] \}, \\ \Delta\nu_{probe}^{2q} &\approx -\Delta\nu_{pump}^{2q}.\end{aligned}\tag{5}$$

As mentioned in Section II, the $\delta\nu_{sps}$ value is generally expected to be small compared to the cavity \mathcal{FSR} value. For our ring cavity, $\delta\nu_{sps}$ (32.6 MHz) is less than $\frac{1}{10}\mathcal{FSR}$ (443.4 MHz). With $\Delta\nu \sim 97\mathcal{FSR}$ and $\delta\nu_{sps} \sim 0$, the $\Delta\nu_{pump}^{sw}$ and $\Delta\nu_{pump}^{2q}$ values determined from Eqs. 4 and 5 agree with the approximate pump detuning values observed in the experiments.

As can be seen in our simulations in Figs. 3b and 4b, our model successfully reproduces the co-existence of the stepwise and coherent two-quantum resonances in the observed two-color

spectra, as well as their linewidths and peak frequency values. However, it fails to reproduce the observed asymmetry in the peak intensities between the red- *vs.* blue-detuned stepwise resonances which occur with similar magnitude of pump-detuning (but opposite in sign). For example, our model predicts that the two stepwise resonant peaks with -655 MHz and $+635$ MHz pump detunings (indicated by the downward-pointing arrows in Figs. 3 and 4) should have similar intensities, due to their nearly equal pump detuning magnitudes. As can be seen in Figs. 3a and 4a, the intensities of these two stepwise peaks are noticeably different, e.g., the stepwise peak at -655 MHz pump detuning in Fig. 3a is more than twice the intensity of the stepwise peak at $+635$ MHz. The degree of asymmetry increases as pressure increases, as can be seen in Fig. 5a, where the intensity ratios between these two stepwise peaks are shown at four pressures. For the narrow, coherent two-quantum peaks, the asymmetry is not observed, e.g., the blue-detuned peak indicated by the magenta asterisk in Fig. 3a is of about the same intensity as the corresponding red-detuned peak indicated by the red asterisk, in agreement with our simulation.

We believe that the failure of our simulation to reproduce the observed red/blue asymmetries among the step-wise, two-color resonance peaks is due to two limits of our model described in Section III: the assumption of a three-level system and our treatment of colli-

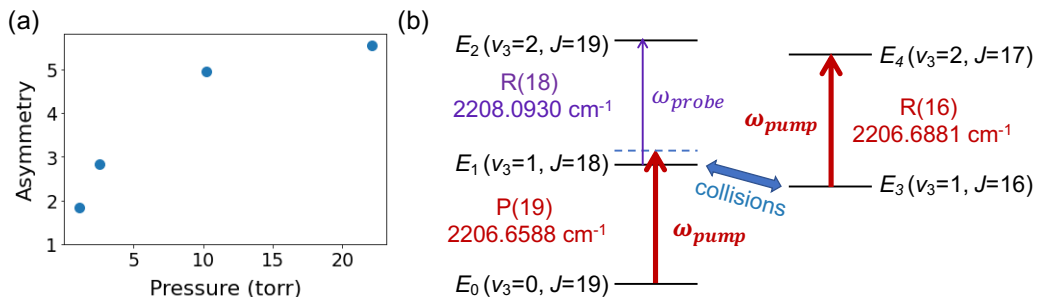


FIG. 5: Illustrations for the origin of the red/blue asymmetry. (a) The asymmetry, defined as the ratio of the -655 MHz and $+635$ MHz pump-detuned peak intensities, is shown as a function of pressure. (b) Level diagram which includes the collision-assisted excitation of the $2 - 1$, R(16) transition by the pump radiation. Collision-induced population transfer between the $\nu_3 = 1$, $J = 18$ level and the $\nu_3 = 1$, $J = 16$ level is indicated by the two-headed arrow. Note that the pump radiation is in resonance with the $2 - 1$, R(16) transition when it is $+890$ MHz blue-detuned from the $1 - 0$, P(19) transition.

sional relaxation. In our three-level-system model (Fig. 1a), the pump laser is assumed to excite only the $1 - 0$, P(19) transition ($2206.6589 \text{ cm}^{-1}$). In reality, the pump radiation, when it is +890 MHz blue-detuned from this target $1 - 0$, P(19) transition, is inadvertently on-resonance with the $2 - 1$, R(16) transition ($2206.6881 \text{ cm}^{-1}$).^{13,14} Facilitated by efficient collisional population transfer from the initial, pump-populated $\nu_3 = 1$, $J = 18$ level to the $\nu_3 = 1$, $J = 16$ level, the $2 - 1$, R(16) transition can be excited by the pump radiation, even though it does not share a common level with the $1 - 0$, P(19) pump transition (see Fig. 5b). The excitation probability for the $2 - 1$, R(16) transition is highest when the pump radiation is +890 MHz *blue*-detuned from the $1 - 0$, P(19) pump transition. We believe that this dual-excitation for a blue-detuned pump is the origin of the observed red *vs.* blue asymmetry. For the coherent two-quantum peaks, since the $\nu_3 = 1$ level is not directly populated, these Doppler-free peaks are not expected to be significantly affected by this additional light-assisted collisional pathway out of the physical $\nu_3 = 1$ level, in agreement with our experimental observations (i.e. the absence of red *vs.* blue asymmetry among the Doppler-free peaks). Details of the five-level model, which includes the collision-induced, $2 - 1$, R(16) pump excitation and a slow-decaying $\nu_3 = 1$ bath, are discussed in the Supplemental Information. This improved treatment for the collisional effects leads to more accurate simulation of the intensity patterns in the observed two-color spectra, e.g., the pressure-dependent asymmetry for the stepwise peaks. Further improvements to the five-level model can be made with incorporation of the laser polarization effect and the Gaussian radial beam profile, and use of more accurate collision-induced population transfer rates between the pump-populated $\nu_3 = 1$ levels and other levels within the $\nu_3 = 1$ rotational manifold. We have plans to experimentally measure the population distribution among the $\nu_3 = 1$ rotational levels under strong pump radiation. Information about this population distribution could be utilized to determine the collision-induced transfer rates within the $\nu_3 = 1$ manifold, with the assumption that the system reaches a steady state under the pump radiation.

B. Background compensation capability

The background compensation capability of our two-color detection with the 1:1 pump switching is shown in Fig. 6. In Fig. 6a, both pump-on and pump-off spectra are shown

in the vicinity of a coherent, two-quantum resonance (2.6 torr). Note that the intensity of this Doppler-free, two-color peak (the same peak as indicated by the red asterisk in Fig. 3a) is more than ten times weaker than that of the strongest stepwise, two-color peak observed under the same pressure (indicated by the upward-pointing arrows in Fig. 3a). The combination of the weak peak intensity and narrow linewidth of this coherent, two-quantum resonance allows a clear demonstration of the frequency-domain background compensation capability of our technique. As can be seen in Fig. 6a, frequency-dependent background wiggles (e.g. the hump near -100 MHz pump detuning) show up in both the pump-on and pump-off spectra. The difference between these two spectra (Fig. 6b) gives the N_2O -induced, two-color spectrum which is free of these large background fringes. The residual noise in the baseline of Fig. 6b can be reduced by longer averaging (1-s averaging is used to record the spectrum in Fig. 6a). In addition to accounting for frequency-dependent empty-cavity decay rates, the time variations of the decay rates are corrected by our two-color detection scheme. In Figs. 6c and 6d, the two-color signals (30 torr) at the top of the Doppler-broadened feature with $+200$ MHz pump detuning are shown over a 30-min period. In our current setup, neither the cavity pressure nor temperature is actively stabilized. To avoid significant laser frequency drift due to the cavity length change (as a result of the pressure and temperature variations), the cavity is loosely locked (± 2 MHz tolerance) to the 10-s running average of the desired molecular beatnote. As can be seen in Fig. 6c, our 1:1 pump switching method allows cancellation of both the short-term variations in the empty-cavity decay rates (e.g. the small spikes in Fig. 6c), and the relatively long-term drift (e.g. the slow drift down).

We must admit that, while the net γ_g signal in Fig. 6d appears relatively flat, there still appears to be some long-term drift in the net signal, as is reflected in its Allan deviation measurement, which has a minimum (0.38 s^{-1}) at 8 min (Fig. 6e). It is likely that the “noisy” flow-through condition, such as variations in the gas flow rate (which affect both the pressure and the N_2O concentration in the cavity), might have contributed to this long-term drift. Based on the Allan deviation measurement in Fig. 6e, the detection limit of our current two-color CRD setup is estimated to be $1 \times 10^{-11} \text{ cm}^{-1}$, or 200 ppq of N_2O (30 torr). This level of sensitivity should be in principle sufficient for two-color measurement of $^{14}\text{CO}_2$ samples with concentrations below the ^{14}C natural abundance (~ 1200 ppq), considering that the transition probabilities for the $^{14}\text{CO}_2$, $\nu_3 = 1-0$ and $\nu_3 = 2-1$ ro-vibrational transitions

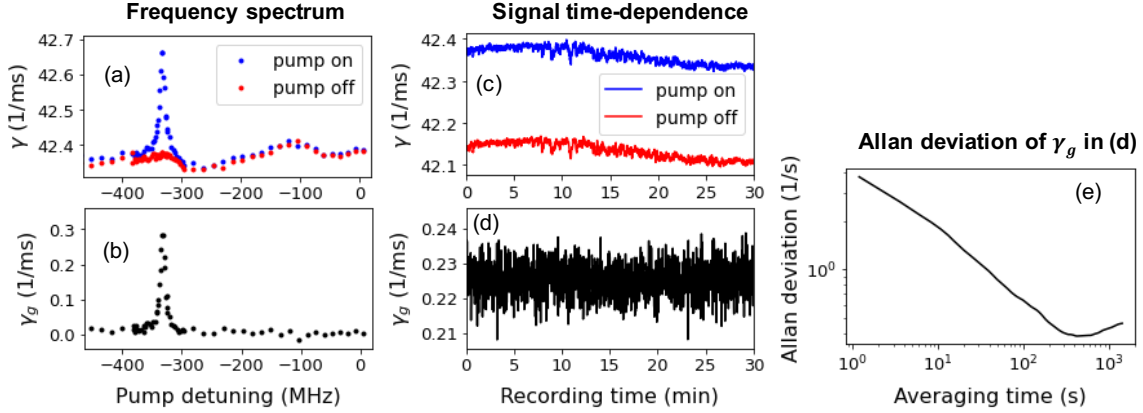


FIG. 6: Background compensation capability. (a) and (b) two-color spectra collected at 2.6 torr. The spectrum in (b) shows the net two-color signals, i.e., the difference between the pump-on and pump-off signals in (a). (c) and (d) time variations of the cavity ringdown rates (at 30 torr, with 0.15 ppb N_2O concentration). The net two-color signals of (c) are shown in (d). The Allan deviation of γ_g in panel (d) is shown in (e).

are each about twice as strong as the corresponding ν_3 transitions of N_2O .¹³ Work is under way to construct a better controlled experimental setup for the $^{14}CO_2$ measurements. A static cell measurement is likely needed to achieve longer averaging time and thus better detection sensitivity. In addition, as mentioned in Section II, even with an attenuated (OD=1.2) probe laser beam and a late-gate for the exponential fit, the two-color probe ringdown signal still suffers from power saturation (i.e. non-exponential ringdown decay), particularly at low pressures (2.6 torr). The effect from saturation becomes less obvious for two-color signals at >20 torr, especially when a late-gated fit is implemented. We believe that power saturation is another factor that affects the sensitivity of our current setup, because the lower signal level from the late-gated signal ($\sim 10\times$ weaker than the full signal level) reduces the S/N for a given data collection time. Based on the standard deviation of the last 100 points of a single-shot ringdown trace (25 nW) measured with 2 MHz detection bandwidth (limited by the sampling rate of the oscilloscope), the effective noise-equivalent-power (NEP) of the detection system is estimated to be $14 \text{ pW/Hz}^{1/2}$.^{27,28} This measured detector NEP is significantly higher than the shot noise power density (with a detector quantum efficiency of 0.4) at the beginning of the ringdown transient, $2.5 \text{ pW/Hz}^{1/2}$. Use of a higher-sensitivity mid-IR detection system, e.g., liquid- N_2 -cooled InSb detector with a

detector-noise-limited preamplifier, could potentially alleviate part of the detector sensitivity issue.

Given the capability of our two-color CRD detection to account for both frequency- and time-dependent empty-cavity decay rates, we believe that our method should be well suited for background absorption cancellation (i.e. from overlapping one-color resonances of other molecular species). For three-level systems with metastable intermediate levels (e.g. the $\nu_3 = 1$ levels of N_2O and CO_2), the Doppler-broadened, stepwise resonance peaks are generally expected to be stronger than the Doppler-free peaks (see discussions in Section IV A and Appendix A). In these cases, the stepwise resonances are the preferred choice for two-color detection. To achieve the best signal-to-noise ratio (S/N), it is preferable to use a pump-probe scheme with the least amount of background absorption near the probe frequency of the two-color peak. In reality, this choice could be heavily influenced by the availability of lasers and their limited tuning ranges. In the worst-case scenario of a strong background molecular absorption that overwhelms the signal from the stepwise, two-color peak (which occurs at nearly zero probe detuning), one of the narrow, coherent two-quantum resonances is an alternative probe option to alleviate the effect from a strong background signal, considering that these resonances (such as the two resonances marked by the red and magenta asterisks in Fig. 3a) occur at probe laser frequencies which are several Doppler FWHM away from the $2 - 1$ resonance frequency.

For a pump-probe scheme which involves either a weak pump transition or a short-lived intermediate level, the intensities of the stepwise two-color peaks are expected to decrease due to inefficient $1 - 0$ pumping, especially if these two-color peaks occur at large pump-detuning values. In both cases, if the pump and probe transition frequencies are known (either experimentally or from *ab initio* calculations) with sufficient accuracy, one can choose a cavity length (equivalently, \mathcal{FSR}) for which the stepwise two-color signals are expected at close to zero pump-detuning (for maximum pumping efficiency), i.e., when $\Delta\nu \sim (n + 1/2)\mathcal{FSR} - \delta\nu_{sps}$, according to Eq. 4. In addition, our simulation indicates that the intensities of the coherent, two-quantum transitions are not significantly affected by the short-lived nature of the intermediate level, because the intermediate level is not directly populated in this Raman-type excitation process. The coherent, two-quantum resonance peaks can be utilized when the stepwise peaks are weak due to the short-lived intermediate level.

C. Comparison with other CRD techniques

The two-color, intracavity pump-probe CRD technique introduced in this work has the potential to be utilized as a generally-applicable, high-sensitivity, high-selectivity detection method for any molecules with ro-vibrational transitions. As discussed in the Introduction, due to its one-photon probe nature, SCAR detection is generally not species-selective, and is thus not suitable for trace-detection in the presence of strong overlapping molecular absorption, e.g., room-temperature $^{14}\text{CO}_2$ trace-detection is not feasible with SCAR detection. The 1C2P-CRD technique has, in principle, similar background (i.e. empty cavity + one-photon absorption) compensation capability as our two-color pump-probe detection scheme. However, the detection sensitivity of the 1C2P method is species-dependent, especially for detection of small molecules, because its implementation requires the existence of near-degeneracy in transition frequencies for a pair of linked $1 - 0$ and $2 - 1$ ro-vibrational transitions. In cases where resonance-enhancement could be exploited for 1C2P excitation, the 1C2P-CRD technique offers an attractive alternative detection scheme to our two-color technique, considering the relative experimental convenience and lower cost for the implementation of the 1C2P method, which utilizes one fewer laser. Just as two-color and 1C2P excitation are both widely used for free-space spectroscopic measurements, the cavity-enhanced version of these two detection schemes should be utilized in a complementary manner.

A reduced parameter correlation from our two-color detection is one further potential advantage of our technique over SCAR and 1C2P-CRD detection. In our two-color pump-probe detection, the pump-on and pump-off decay rates are, by design, *un*-correlated, because the pump-on and pump-off signals are separately measured in a 1:1 fashion. As a result, both decay rates can be determined as accurately as the decay rates measured by conventional, unsaturated, one-photon CRD detection. In comparison, both SCAR and 1C2P-CRD detection rely on the ability to determine two types of cavity losses from a *single* decay trace, i.e., saturable (molecular transitions) *vs.* non-saturable (empty cavity + weak molecular transitions) for the former,³⁻⁶ and linear (empty cavity + one-photon-absorption) *vs.* two-photon-induced for the latter technique.¹⁰⁻¹² The two decay rates determined from a single ringdown trace are inevitably correlated in SCAR and 1C2P-CRD detection. Larger parameter correlations leads to larger standard deviations for the fit parameters, which effectively decreases the detection S/N. For example, even under optimal experimental conditions, the

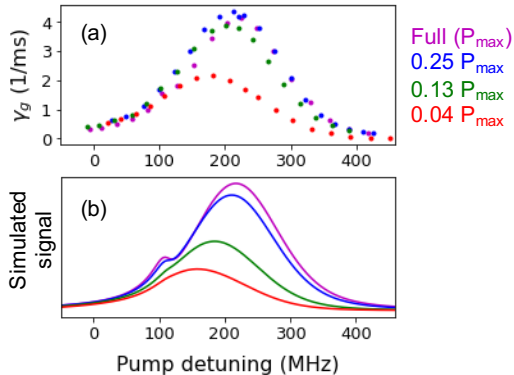


FIG. 7: The dependence of a stepwise, two-color peak on the pump radiation power. (a) and (b) Experimental and simulated spectra at 10.2 torr. The full intracavity pump radiation power is estimated to be 36 W (Section II).

standard deviations of the analyte concentrations from SCAR measurements are about $10\times$ larger than those determined from an exponential decay fit.¹¹

While two-color CRD detection utilizes one more laser than SCAR and 1C2P-CRD detection, there is no substantial technical difficulty in incorporating this additional laser into the detection system, especially with a traveling-wave cavity setup in which the combining/separation of the two orthogonally polarized, counter-propagating laser beams can be easily achieved with a pair of polarizing beam splitters (Fig. 2). The pump and probe beams are *inherently* and *perfectly* overlapped once they are individually coupled into the cavity. Furthermore, as a result of strong saturation of the pump transition, the two-color pump-probe signals are insensitive to changes in the intracavity pump radiation power. As can be seen in Fig. 7a, the intensity of the Doppler-broadened, stepwise peak does not decrease significantly, even with nearly $10\times$ attenuated pump radiation (36 W \rightarrow 4.5 W). An intracavity *p*-mode power of 4.5 W is relatively easy to achieve with most commercial laser systems frequency-locked to a medium finesse cavity ($F = 5000$), even for those with significantly lower output power (5 mW) than our pump QCL (50 mW). The insensitivity of the pump-probe signal to the pump laser power also means that our two-color CRD detection should be relatively immune to small intracavity pump power fluctuations ($\sim 0.5\%$ in our current setup). For 1C2P-CRD detection, a ten-fold decrease in the intracavity laser power would significantly degrade its detection sensitivity and selectivity, considering that the 1C2P absorption coefficient, which has unit of cm^{-1}/W , depends linearly on the laser

power. Similarly, the sensitivity of SCAR detection requires a substantial level of saturation at the beginning of the ringdown.^{11,29} A factor of ten decrease in the saturation could lead to a significant decrease in its sensitivity. As can be seen in Fig. 7b, the insensitivity of the stepwise two-color peak to the pump power (Fig. 7a) is qualitatively captured by our simulation model. For example, the model predicts that with 1/4 of the full pump power, the stepwise peak intensity remains close to that at full power. The model, however, predicts an overall faster decrease in the signal intensity than the experimental observations.

We believe that the experimental flexibility in the selection of the pump-probe schemes is another important feature of our two-color CRD technique. Given the high-finesse and thus long effective absorption pathlength required for high sensitivity detection (7.1 km for the probe in our cavity), even weak absorption features could lead to significant attenuation of the intracavity radiation power. For example, for CO₂ samples at 20 torr and 296 K, transitions with spectral line intensities as low as $1 \times 10^{-26} \text{ cm}^{-1}/(\text{molecule}\cdot\text{cm}^{-2})$ can cause $\sim 20\%$ attenuation in the intracavity probe power in our cavity. In the spectral region of interest for two-color ¹⁴CO₂ detection (e.g. 2190-2215 cm⁻¹, where the $\nu_3 = 2 - 1$ and $1 - 0$ transitions of ¹⁴CO₂ occur), the density of such strongly-attenuating transitions is approximately ten per wavenumber from ¹³CO₂ and ¹²CO₂ alone, and about 10% of these transitions have line intensities $> 1 \times 10^{-24} \text{ cm}^{-1}/(\text{molecule}\cdot\text{cm}^{-2})$. Trace-detection in the vicinity of these strongly-attenuating absorption features is highly undesirable. With careful selection of pump and probe transitions, the effects of these strongly-attenuating absorption features could be minimized with our two-color detection method.

V. CONCLUSION

In this work, we present a proof of principle demonstration of mid-IR, two-color, intracavity, pump-probe CRD detection using a ladder-type, three-level system based on the N₂O $\nu_3 = 1 - 0$, P(19) (pump) and $\nu_3 = 2 - 1$, R(18) (probe) ro-vibrational transitions. We believe that this type of intracavity pump-probe scheme which utilizes strong mid-IR, $1 - 0$ and $2 - 1$ transitions is ideal for high-sensitivity and high-selectivity trace-detection, and to our knowledge, it has not been previously reported in the literature. With dual-frequency-locked pump and probe lasers, we achieve high intracavity pump radiation power (36 W) and > 2 kHz ringdown acquisition rates. The pump radiation is switched off during

every other probe ringdown event. The difference between the pump-on and pump-off decay rates yields the net, two-color-induced absorption signals, which are immune to empty-cavity ringdown fluctuations and spectral overlaps from unwanted, background molecular absorption. Work is under way to build a better controlled experimental setup, with the ultimate goal of room-temperature operation of ^{14}C quantification at sub-natural-abundance levels. The feasibility of our two-color CRD detection under flow-through conditions is also promising for future field-work applications, as well as CRD measurements of combusted samples following HPLC separation.³⁰

Compared to SCAR and 1C2P-CRD detection, we believe that our two-color CRD detection is a more generally applicable high-sensitivity, high-selectivity trace-detection method. The mid-IR, two-color CRD detection scheme is expected to be applicable for essentially any molecular species with mid-IR, ro-vibrational transitions, which are typically strong for at least one of the vibrational modes of the molecule (e.g. the ν_3 anti-symmetric stretch mode for N_2O , CO_2 , C_2H_2 , etc). In comparison, the use of 1C2P-CRD detection is species-dependent, due to the nature of its excitation scheme. The SCAR method, due to its one-photon nature, is not expected to work optimally in the presence of strong absorption from non-target molecular transitions. Furthermore, in our two-color detection, the pump-on and pump-off cavity decay rates are individually determined from two un-correlated measurements. Given that these un-correlated measurements are recorded in quick succession (about every $250 \mu\text{s}$), effective background compensation can be achieved. In comparison, in both SCAR and 1C2P-CRD detection, two decay rates are derived from a single decay trace, which inevitably leads to stronger parameter correlations and consequently larger fit standard deviations than our two-color measurements (e.g. $\sim 10\times$ higher for SCAR).

In addition to its use as a high-sensitivity, high-selectivity trace-detection method, we believe that our mid-IR, pump-probe scheme is well suited for rotation-state-resolved measurements of vibrationally excited states of large and non-volatile molecular species, e.g., with pump and probe at $8.5 \mu\text{m}$, the vibration-rotation structure of the C_{60} fullerene in the 2400 cm^{-1} energy region can be investigated based on the newly observed T_{1u} -symmetry fundamental transitions (i.e. used as the pump transitions).¹⁹ High-resolution spectroscopic studies of these large molecular systems, especially at high internal energies, are challenging both experimentally (e.g. low gas-phase density, detection sensitivity and selectivity)¹⁹ and theoretically (e.g. wide-spread intramolecular vibrational redistribution).³¹ The Doppler-

free, coherent two-quantum resonances observed in our two-color excitation scheme are likely the most suitable transitions for these high-resolution studies, due to their narrow linewidths (FWHM of ~ 15 MHz at 2.5 torr and room temperature) and small AC Stark shifts (~ 2 MHz in our experiment with full pump power). While the accuracy in the transition frequency measurements is not the focus of this work, pump-induced light shifts could be in principle readily accounted for by our simulation model. With the rapid development of mid-IR radiation sources and multi-channel detectors,³² one potential extension of our mid-IR pump-probe scheme is the use of broadband radiation as the probe, such as a mid-IR frequency-comb (i.e., QCL-pumped, frequency-comb-probed, CRD detection) to achieve rapid, multiplexed detection with high sensitivity and selectivity.³³

Supplementary Material

See the supplemental material for details of the five-level simulation and the experimental observations of collision-induced, two-color transitions.

Corresponding Author

*mccartt1@llnl.gov

Acknowledgments

The authors would like to thank Professor Robert W. Field (MIT) and Dr. Stephen L. Coy (MIT) for their critical comments on this manuscript. The authors are grateful to Reviewer 1 for providing insights to this project. Research reported in this publication was supported by the National Institute Of General Medical Sciences of the National Institutes of Health under Award Number R01GM127573. The content is solely the responsibility of the authors and does not necessarily represent the official views of the National Institutes of Health. Work performed in part at the National User Resource for Biological Accelerator Mass Spectrometry, which is operated at LLNL under the auspices of the U.S. Department of Energy under contract DE-AC52-07NA27344. The User Resource is supported by the National Institutes of Health, National Institute of General Medical Sciences under grant

Data Availability Statements

The data that support the findings of this study are available from the corresponding author upon reasonable request.

APPENDIX A: COLLISIONAL EFFECTS

In our simulation, we are only able to reproduce the relative intensities of the broad stepwise resonances and the Doppler-free, coherent two-quantum resonances by using a significantly slower population decay rate (γ) than the coherence decay rate (γ_{ij}), i.e., $\frac{\gamma_{ij}}{\gamma} = 100$. As discussed in Section IV A, the $1 - 0$ transition is strongly saturated, with a power-broadened FWHM of ~ 1 GHz. For a two-level system, the homogeneous linewidth (i.e. from collisions and power-broadening) is proportionally to $\sqrt{\gamma_{ij}^2 + 4(\frac{\gamma_{ij}}{\gamma})\Omega_{ij}^2}$.²³ While a large pump Rabi-frequency ($2\Omega_{10}$) alone could result in a large power-broadened $1 - 0$ linewidth, the simulated spectra under this assumption ($\frac{\gamma_{10}}{\gamma} \sim 1$ and $\frac{\Omega_{10}}{2\pi} \sim 250$ MHz) would become *overwhelmingly* dominated by the Doppler-free, coherent two-quantum peaks. Only the choice of a moderately large $\frac{\Omega_{10}}{2\pi}$ value (25 MHz) in combination with a slow population decay rate yields a simulation that qualitatively reproduces the observed experimental features.

We believe that the slower than expected population decay rate required for the success of our simulation model is a consequence of the phenomenological manner in which the collisional effects are treated—in particular for the population decay from the $\nu_3 = 1$, $J = 18$ and $\nu_3 = 2$, $J = 19$ levels (Fig. 1a). While the J - and m -changing collisions are expected to be fast (~ 10 ns lifetime at 10 torr), the $\nu_3 = 1$ level of N_2O is known to have long vibrational relaxation time ($21 \mu\text{s}$ for collisions with N_2 at 10 torr), based on time-resolved mid-IR fluorescence measurements.^{24,25} As a result of this long relaxation time, the rotational population can be trapped within the $\nu_3 = 1$ manifold for much longer than the average collisional period. In the presence of the strong pump radiation, significant population exists not only in the $\nu_3 = 1$, $J = 18$ level which is directly populated by the pump radiation, but also in other levels within the $\nu_3 = 1$ rotational manifold which are populated through rotational population transfer from $\nu_3 = 1$, $J = 18$. The *bi*-directional interaction between

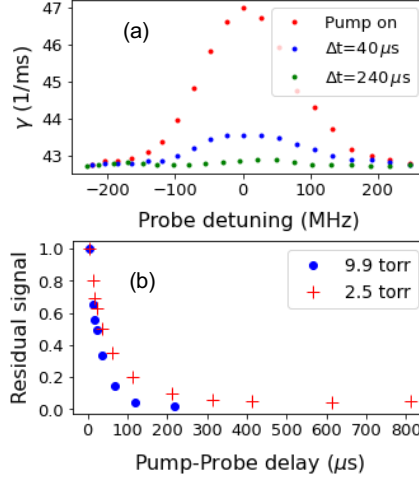


FIG. 8: The residual pump-off signals. (a) The pump-on signals, and the residual pump-off signals at two pump-probe delay time. The spectra are taken at 2.5 torr. (b) The magnitude of the residual signals as a function of pump-probe delay time at two different pressures.

the pump-populated $\nu_3 = 1$, $J = 18$ level and the $\nu_3 = 1$ rotational manifold “bath” can thus no longer be neglected in our excitation scheme. For simplicity, this *bi*-directional energy flow is not considered in our three-level model, for which both level 1 and 2 are assumed to decay, *uni*-directionally, to a common bath. We believe that the population decay rate used in our simplified three-level model should be considered an effective, *net* decay rate which phenomenologically describes the *bi*-directional population flow from level 1 and 2 to their respective ν_3 -baths. The *bi*-directional population exchange between $\nu_3 = 1$, $J = 18$ and the $\nu_3 = 1$ rotational manifold is included in our five-level-system model, discussed in the Supplemental Information.

We have observed, using our two-color CRD detection, evidences that support the long ensemble lifetime of the $\nu_3 = 1$ level. Due to the high energy of the $\nu_3 = 1$ level ($\sim 2200 \text{ cm}^{-1}$), the $2 - 1$, R(18) probe transition cannot be observed in the absence of the pump (i.e. pump-off for the entire experiment). In our 1:1 pump switching experiments, we nevertheless observe the $2 - 1$, R(18) transition when the pump radiation is shut off close to the start of probe ringdown, e.g., a pump-probe delay (Δt) less than $50 \mu s$. In Fig. 8a, the pump-on and pump-off signals with two different Δt are shown in the vicinity of a stepwise, two-color resonance (2.5 torr). As discussed in Section IV A, the stepwise two-color resonances always occur with close to zero probe detuning. As can be seen in Fig. 8a, with $\Delta t = 40 \mu s$, we

still observe a strong probe absorption signal at the $2 - 1$, R(18) transition frequency. This suggests that a significant portion of the pump-excited, $\nu_3 = 1$, $J = 18$ population remains in the same state after the pump radiation has been off for $40 \mu\text{s}$. In Fig. 8b, the magnitudes of this residual signal are shown, as a function of Δt , at 2.5 and 9.9 torr. As can be seen in Fig. 8b, the residual signals decay faster at the higher pressure ($49 \pm 8 \mu\text{s}$ and $27 \pm 6 \mu\text{s}$, respectively, at 2.5 and 9.9 torr). While the measured decay time at 9.9 torr is in good agreement with the measurements in Ref. [24] for N_2O collisions with N_2 , the decay time at 2.5 torr is only $\sim 60\%$ of the measured value. Considering that the diffusion time of N_2O in N_2 is expected to be $\sim 40 \mu\text{s}$ for a distance of 0.8 mm (the beam radius) at 2.5 torr,³⁴ diffusion of the pump-excited N_2O molecules out of the laser beam likely contributes to this observed discrepancy.

-
- ¹ D. Romanini, I. Ventrillard, G. Méjean, J. Morville, and E. Kerstel, in *Cavity-enhanced Spectroscopy and Sensing*, edited by G. Gagliardi and H.-P. Loock (Springer, 2014) Chap. 1, pp. 1–51.
- ² S. Welzel, R. Engeln, and R. J., in *Cavity-enhanced Spectroscopy and Sensing*, edited by G. Gagliardi and H.-P. Loock (Springer, 2014) Chap. 3, pp. 93–142.
- ³ G. Giusfredi, S. Bartalini, S. Borri, P. Cancio, I. Galli, D. Mazzotti, and P. De Natale, *Physical Review Letters* **104**, 110801 (2010).
- ⁴ I. Galli, S. Bartalini, S. Borri, P. Cancio, D. Mazzotti, P. De Natale, and G. Giusfredi, *Physical Review Letters* **107**, 270802 (2011).
- ⁵ G. Giusfredi, I. Galli, D. Mazzotti, P. Cancio, and P. De Natale, *Journal of the Optical Society of America B* **32**, 2223 (2015).
- ⁶ I. Galli, S. Bartalini, R. Ballerini, M. Barucci, P. Cancio, M. De Pas, G. Giusfredi, D. Mazzotti, N. Akikusa, and P. De Natale, *Optica* **3**, 385 (2016).
- ⁷ A. D. McCartt, T. J. Ognibene, G. Bench, and K. W. Turteltaub, *Analytical Chemistry* **88**, 8714 (2016).
- ⁸ A. J. Fleisher, D. A. Long, Q. Liu, L. Gameson, and J. T. Hodges, *The Journal of Physical Chemistry Letters* **8**, 4550 (2017).
- ⁹ N. A. Kratochwil, S. R. Dueker, D. Muri, C. Senn, H. Yoon, B.-Y. Yu, G.-H. Lee, F. Dong, and M. B. Otteneder, *Plos one* **13**, e0205435 (2018).
- ¹⁰ K. K. Lehmann, *The Journal of Chemical Physics* **151**, 144201 (2019).
- ¹¹ K. K. Lehmann, *Applied Physics B* **116**, 147 (2014).
- ¹² G. Zhao, D. M. Bailey, A. J. Fleisher, J. T. Hodges, and K. K. Lehmann, *Physical Review A* **101**, 062509 (2020).
- ¹³ I. E. Gordon, L. S. Rothman, C. Hill, R. V. Kochanov, Y. Tan, P. F. Bernath, M. Birk, V. Boudon, A. Campargue, K. Chance, *et al.*, *Journal of Quantitative Spectroscopy and Radiative Transfer* **203**, 3 (2017).
- ¹⁴ R. Toth, see <http://mark4sun.jpl.nasa.gov/data/spec/N2O> (2004).
- ¹⁵ E. J. Zak, J. Tennyson, O. L. Polyansky, L. Lodi, N. F. Zobov, S. A. Tashkun, and V. I. Perevalov, *Journal of Quantitative Spectroscopy and Radiative Transfer* **189**, 267 (2017).

- ¹⁶ I. Galli, P. C. Pastor, G. Di Lonardo, L. Fusina, G. Giusfredi, D. Mazzotti, F. Tamassia, and P. De Natale, *Molecular Physics* **109**, 2267 (2011).
- ¹⁷ J. Karhu, K. Lehmann, M. Vainio, M. Metsälä, and L. Halonen, *Optics Express* **26**, 29086 (2018).
- ¹⁸ C.-L. Hu, V. I. Perevalov, C.-F. Cheng, T.-P. Hua, A.-W. Liu, Y. R. Sun, Y. Tan, J. Wang, and S.-M. Hu, *The Journal of Physical Chemistry Letters* **11**, 7843 (2020).
- ¹⁹ P. B. Changala, M. L. Weichman, K. F. Lee, M. E. Fermann, and J. Ye, *Science* **363**, 49 (2019).
- ²⁰ R. Drever, J. L. Hall, F. Kowalski, J. Hough, G. Ford, A. Munley, and H. Ward, *Applied Physics B* **31**, 97 (1983).
- ²¹ S. Saraf, R. L. Byer, and P. J. King, *Applied Optics* **46**, 3850 (2007).
- ²² T. Schmalz and W. Flygare, in *Laser and Coherence Spectroscopy* (Springer, 1978) pp. 125–196.
- ²³ R. L. Shoemaker, in *Laser and Coherence Spectroscopy*, edited by J. I. Steinfeld (Springer, 1978) Chap. 3, pp. 197–371.
- ²⁴ H. Gueguen, F. Yzambart, A. Chakroun, M. Margottin-Maclou, L. Doyennette, and L. Henry, *Chemical Physics Letters* **35**, 198 (1975).
- ²⁵ K. L. Poel, Z. T. Alwahabi, and K. D. King, *The Journal of Chemical Physics* **105**, 1420 (1996).
- ²⁶ S. Bauer, J. Caballero, R. Curtis, and J. Wiesenfeld, *Journal of Physical Chemistry* **91** (1987).
- ²⁷ H. Huang and K. K. Lehmann, *The Journal of Physical Chemistry A* **117**, 13399 (2013).
- ²⁸ K. K. Lehmann and H. Huang, in *Frontiers of Molecular Spectroscopy* (Elsevier, 2009) pp. 623–658.
- ²⁹ I. Sadiq and G. Friedrichs, *Physical Chemistry Chemical Physics* **18**, 22978 (2016).
- ³⁰ A. T. Thomas, T. Ognibene, P. Daley, K. Turteltaub, H. Radousky, and G. Bench, *Analytical Chemistry* **83**, 9413 (2011).
- ³¹ D. J. Nesbitt and R. W. Field, *The Journal of Physical Chemistry* **100**, 12735 (1996).
- ³² M. L. Weichman, P. B. Changala, J. Ye, Z. Chen, M. Yan, and N. Picqué, *Journal of Molecular Spectroscopy* **355**, 66 (2019).
- ³³ M. J. Thorpe, K. D. Moll, R. J. Jones, B. Safdi, and J. Ye, *Science* **311**, 1595 (2006).
- ³⁴ D. Pritchard and J. Currie, *Journal of Soil Science* **33**, 175 (1982).